Exploring the orbital alignments of Galactic close white dwarf binaries with LISA

Naoki Seto

Department of Physics, Kyoto University, Kyoto 606-8502, Japan

(Received 15 February 2024; accepted 9 April 2024; published 13 May 2024)

Using the proposed space gravitational wave detector LISA, we will be able to measure the geometrical configurations of $\sim 10^4$ close white dwarf binaries in our Galaxy. The obtained data will be an entirely new resource to examine the randomness of their orbital orientations. Partly motivated by a recent reported on the systematic alignments of bulge planetary nebulae, we discuss the outlook of the orientational analysis with LISA. We find that a quadrupole pattern as small as ~ 0.05 can be detected for bulge white dwarf binaries, owing to their large available number. From such a pattern analysis, we might geometrically explore fossil records in our Galaxy billions of years ago.

DOI: 10.1103/PhysRevD.109.103016

I. INTRODUCTION

Since 2015, the LIGO-Virgo-Kagra network has detected gravitational wave (GW) signals from ~ 100 merging extra-Galactic binaries in the 10–1000 Hz band [1–3]. Quite recently, in the nHz band, various theoretical models have been actively discussed with the advent of new pulsar timing data [4–7]. In the 2030s, the Laser Interferometer Space Antenna (LISA) will be launched and will explore GWs around 0.1–100 mHz [8]. LISA has the potential to observe massive black holes at cosmological distances, although the estimated detection rates have large uncertainties [8].

More securely, LISA will separately detect $\sim 10^4$ close white dwarf binaries (CWDBs) in our Galaxy, as nearly monochromatic GW sources [8–12]. Indeed, for improving the effective sensitivity of LISA, it is essential to identify these vast number of binaries and subtract their foreground GW signals [13]. A significant fraction ($\sim 30\%$) of the identified CWDBs will be the bulge component, located near the Galactic center [14]. The remaining ones will be distributed more broadly around the Galactic disk. In both cases, the orbital motions of the CWDBs are directly encoded in the emitted GW signals [15–17]. Using LISA, we can receive the GW signals, decode them and generate a long and high-quality list for the orbital configurations of the CWDBs, solely based on the first principles of physics. Note that most of CWDBs are expected to have negligible eccentricities due to tidal effects (as for the known CWDBs [8,12]).

In relation to the orientations (i.e., the directions of angular momentum vectors) of CWDBs, on the basis of electromagnetic observations, there recently appeared an interesting report on the bulge planetary nebulae (PNe) which are (or are inferred to be) specifically associated with short-period ($\lesssim 1$ day) binaries (in total of 14 systems) [18]. In contrast to the whole bulge PN populations, the orientations of the symmetric axes of the specific PNe show concentrations nearly parallel to the Galactic plane, at 5σ significance. PNe are ionized gas ejected at the formation of white dwarfs [19] and closely related to the common envelope phases [20]. In the report, the orientations of the specific subset are considered to be parallel to the orbital angular momentum vectors of the associated short-period binaries (see also [21]). Then, the angular momentum vectors of the binaries are not randomly oriented but more probable to be nearly parallel to the Galactic disk (roughly speaking, removing PNe from the triple geometrical relations between the short-period binaries, PNe and the Galactic plane). In general, binary formation should involve various physical processes and could also depend on time and location [22]. The reported alignments might be embedded already at the formations of the bulge binaries billions of years ago, e.g., due to ordered strong magnetic fields as argued in the report [18].

Regarding the potential alignments of compact binaries in the bulge, we await further studies, in particular, independent observational analyses (see also [23] for nearby binaries). Here the long list of CWDBs provided by LISA could be an invaluable and solid resource. With the large number of the available sample, we will be able to detect a weak anisotropic pattern existing in their orientation distribution function.

In this work, we discuss the outlook of such an inquiry with LISA, paying special attentions to the geometrical aspects of the involved systems. Along the way, we point out a fourfold degeneracy at determining the polarization angle ψ, which fixes the binary's orientation around the line-of-sight direction. This degeneracy is induced by the underlying symmetry of the measurable gravitational

waveform and can be effectively regarded as an irreversibility in the information transfer (from the encoding to the decoding), partially hampering our observational analysis. For the data analysis of actual CWDB sample, we examine a simple dualistic approach to statistically enhance its anisotropic pattern. The associated detection limit can be as small as ∼0.05 for a quadupole mode of the spherical harmonic expansion. Through this pattern analysis, LISA might enable us to geometrically delve into the ancient history of our Galaxy.

II. ORIENTATIONS OF CWDBS

A. Axisymmetric model

As shown in Fig. 1, we first define the relevant unit vectors for describing the configuration of a circular CWDB. We put its sky direction $\vec{n}$ and its orientation $\vec{j}$ (parallel to its angular momentum vector). We also set $\vec{q}$ as the direction of the Galactic rotation axis. The Galactic plane is normal to $\vec{q}$.

Given the recent report on the bulge PNe [18], we are primarily interested in the probability distribution function $\mathcal{P}(\vec{j})$ for the orientations $\vec{j}$ of the bulge CWDBs, in particular, its pattern relative to the rotation axis $\vec{q}$. We thus set $\vec{q}$ as the polar direction for the spherical harmonic bases $Y_{lm}(\vec{j})$.

We assume that the function $\mathcal{P}(\vec{j})$ is axisymmetric around the vector $\vec{q}$. Then the function $\mathcal{P}(\vec{j})$ depends only on the polar angle θ (i.e., only with $m = 0$ modes). Given the normalization condition, the resultant axisymmetric function is expanded as

$$\mathcal{P}_A(\cos\theta) = (4\pi)^{-1/2}[Y_{00}(\theta) + a_{10}Y_{10}(\theta) + a_{20}Y_{20}(\theta) + a_{30}Y_{30}(\theta) + a_{40}Y_{40}(\theta) + \cdots], \quad (1)$$

defined in the range $0 \le \theta \le \pi$. We have $Y_{l0}(\theta) \propto L_l(\cos\theta)$ with the Legendre polynomials $L_l(x)$ (in an unconventional notation to prevent confuses with probability distribution functions), which satisfy the odd-even identities

$$L_l(-x) = (-1)^l L_l(x). \quad (2)$$

We present some of the explicit forms $Y_{00} = (4\pi)^{-1/2}$, $Y_{10} \propto \cos\theta$, $Y_{20} \propto (3\cos^2\theta - 1)/2$, $Y_{30} \propto (5\cos^3\theta - 3\cos)/2$, and $Y_{40} \propto (35\cos^4\theta - 30\cos^2\theta + 3)/8$. For a even l, we have $Y_{l0}(0) = Y_{l0}(\pi) > Y_{l0}(\pi/2)$, and a negative value a_{l0} resultantly induces a higher concentration to the equatorial directions ($\theta = \pi/2$) rather than the polar directions. We have $\mathcal{P}(\vec{j}) = 1/(4\pi)$ for the isotropic (random) orientation distribution with $a_{10} = a_{20} = \cdots = 0$. Later, in Sec. III, we will discuss which parameters a_{l0} we can determine for the Galactic CWDBs with LISA.

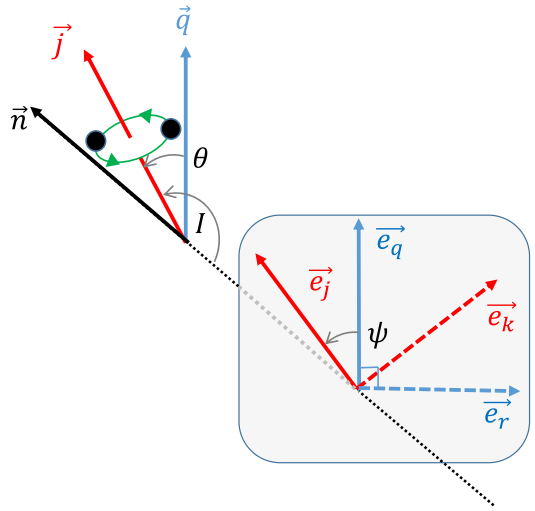

FIG. 1. Schematic picture for a binary configuration. All the seven vectors are unit vectors. The vectors $\vec{n}$ and $\vec{j}$ represent the direction and orientation of the binary. The Galactic plane is normal to the vector $\vec{q}$. The angles I and θ are respectively between $\vec{j}$-$(-\vec{n})$ and $\vec{j}$-$\vec{q}$. The gray plane is normal to the line-of-sight direction $\vec{n}$, and the vectors $\vec{e}_j$ and $\vec{e}_q$ are the projections of $\vec{j}$ and $\vec{q}$, with the polarization angle ψ between them. The two remaining vectors $\vec{e}_k$ and $\vec{e}_r$ are respectively perpendicular to $\vec{e}_j$ and $\vec{e}_q$.

B. Coordinate transformation

For discussing GW observation, it is convenient to introduce the two unit vectors $(\vec{e}_j, \vec{e}_k)$ normal to the binary direction $\vec{n}$ (see Fig. 1). Here the unit vector $\vec{e}_j$ shows the transverse projection of the orientation vector $\vec{j}$, with the remaining one $\vec{e}_k (= \vec{n} \times \vec{e}_j)$.

The unit vector $\vec{e}_q$ is similarly defined by the transverse projection of $\vec{q}$ with $\vec{e}_r (= \vec{n} \times \vec{e}_q)$. For a given binary direction $\vec{n}$, the vectors $\vec{e}_q$ and $\vec{e}_r$ are fixed, and we can specify the orientation $\vec{j}$ in terms of the inclination angle I and the polarization angle ψ (see Fig. 1). We have the following relations:

$$\vec{e}_k = \vec{e}_r\cos\psi + \vec{e}_q\sin\psi, \qquad \vec{e}_j = -\vec{e}_r\sin\psi + \vec{e}_q\cos\psi. \quad (3)$$

Our next task is to generate the distribution function $p(I, \psi)$ given in the observer's frame, using the aforementioned one $\mathcal{P}_A(\cos\theta)$ given in the Galactic frame. To this end, we first discuss the mismatch between $\vec{q}$ and $\vec{e}_q$. Our solar system is almost on the mid-Galactic plane. The distance to the bulge is ∼8.3 kpc and its scale height is ∼0.5 kpc [24]. Therefore, the vector $\vec{q}$ is nearly normal to $\vec{n}$, and we have $\vec{q} \simeq \vec{e}_q$ with the typical mismatch angle (in radians) $\gamma \sim 0.5/8.3 \ll 1$. We then have

$$\cos\theta = \vec{j}\cdot\vec{q} \simeq \vec{j}\cdot\vec{e}_q = \sin I\cos\psi \quad (4)$$

and correspondingly

$$p(I,\psi) \simeq \mathcal{P}_A(\sin I \cos\psi). \tag{5}$$

Below, we apply equalities to the relations (4) and (5) (a distant observer approximation). It is a straightforward but cumbersome task to derive the function $p(I,\psi)$ without the approximation. Importantly, our approximation does not introduce artificial anisotropies to $p(I,\psi)$ from the originally isotropic function $\mathcal{P}(\vec{j}) = 1/(4\pi)$. In terms of the harmonic expansion $p(I,\psi) = \sum_{lm} b_{lm} Y_{lm}(I,\psi)$, the coefficients b_{lm} at $l \lesssim 1/\gamma \sim 15$ will be virtually unaffected by our approximation (i.e. ignorable at the lower degrees such as $l \lesssim 4$). Geometrically, Eq. (5) can be regarded as a 90° rotation of the polar direction (from $\theta = 0$ to $I = 0$), thus keeping the degrees l at the correspondence of their expansion coefficients (see e.g., [25]). Even if we start from an axisymmetric model $\mathcal{P}_A(\cos\theta)$ as in Eq. (1), the transformed one $p(I,\psi)$ can depend on the polarization (azimuthal) angle ψ.

III. GW OBSERVATION

A. Waveform model

We now focus on a nearly monochromatic GW from a circular CWDB with an orbital frequency $f/2$. We keep the essential aspects for our study, dropping irrelevant details.

In the lowest quadrupole approximation, the gravitational waveform at a given position is expressed as

$$\begin{aligned}\boldsymbol{h}(t,\vec{n},I,\psi) = {} & A_+(I)\cos(2\pi f t+\alpha)\mathbf{e}_+(\vec{n},\psi) \\ & + A_\times(I)\sin(2\pi f t+\alpha)\mathbf{e}_\times(\vec{n},\psi),\end{aligned} \tag{6}$$

with the phase constant α and the two amplitudes $A_+(I) \propto (1+\cos^2 I)$ and $A_\times(I) \propto 2\cos I$ (see e.g., [15]). The transverse-traceless tensors $\boldsymbol{e}_{+,\times}(\vec{n},\psi)$ are given by

$$\boldsymbol{e}_+(\vec{n},\psi) = \vec{e}_k \otimes \vec{e}_k - \vec{e}_j \otimes \vec{e}_j, \quad \boldsymbol{e}_\times(\vec{n},\psi) = \vec{e}_k \otimes \vec{e}_j + \vec{e}_j \otimes \vec{e}_k \tag{7}$$

with the vectors $\vec{e}_k$ and $\vec{e}_j$ defined in Eq. (3).

From Eqs. (3) and (7), we readily obtain the identities $\mathbf{e}_{+,\times}(\vec{n},\psi+\pi) = \mathbf{e}_{+,\times}(\vec{n},\psi)$ and resultantly,

$$\boldsymbol{h}(t,\vec{n},I,\psi+\pi) = \boldsymbol{h}(t,\vec{n},I,\psi). \tag{8}$$

This degeneracy between ψ and $\psi+\pi$ is fundamental, originating from the spin-2 nature of the gravitational radiation.

From Eqs. (3) and (7), we can also confirm the identities $\mathbf{e}_{+,\times}(\vec{n},\psi+\pi/2) = -\mathbf{e}_{+,\times}(\vec{n},\psi)$ and thus,

$$\boldsymbol{h}(t,\vec{n},I,\psi+\pi/2) = -\boldsymbol{h}(t,\vec{n},I,\psi), \tag{9}$$

(see e.g., [26,27]). Correspondingly, the $\pi/2$- rotation of the polarization angle ψ can be effectively absorbed by the phase shift $\alpha+\pi$ in Eq. (6). Therefore, we observationally have the degeneracy between ψ and $\psi+\pi/2$ at the lowest Newtonian order. By observing the higher post-Newtonian waveforms at frequencies $f/2$ and $3f/2$ and measuring their phases relative to that of the Newtonian one (6), we can, in principle, distinguish the two states at ψ and $\psi+\pi/2$ [see e.g., Eq. (11.295b) in [15]]. Unfortunately, compared with the Newtonian waveform (6), the higher ones are suppressed by the post-Newtonian parameter $\beta = O(c^2/v^2)$. For our CWDBs, we have

$$\beta = \left(\frac{\pi G M_t f}{c^3}\right)^{2/3} \sim 10^{-5}\left(\frac{f}{5\ \mathrm{mHz}}\right)^{2/3}\left(\frac{M_t}{1M_\odot}\right)^{2/3} \tag{10}$$

where M_t is the total mass of the binary. Unlike binary black hole mergers observed by ground-based detectors (see e.g., [28]), the small post-Newtonian waveforms of the CWDBs are easily masked by the measurement noises, and we cannot practically solve the degeneracy between ψ and $\psi+\pi/2$. From Eqs. (8) and (9), we have a similar degeneracy between ψ and $\psi+3\pi/2$.

In summary, GW observation is a geometrical measurement and intrinsically has a good affinity for studying the configurations of the Galactic CWDBs. However, because of the symmetry of the system, we have the fourfold degeneracy between the angles $\psi, \psi+\pi/2, \psi+\pi$, and $\psi+3\pi/2$.

B. Fourfolded distribution function

As discussed in the previous subsection, our observable is not the full distribution function $p(I,\psi)$ but the folded one,

$$\bar{p}(I,\psi_d) \equiv \sum_{k=0}^{3} p(I,\psi_d + k\pi/2), \tag{11}$$

defined in the parameter ranges $0 \le I \le \pi$ and $0 \le \psi_d \le \pi/2$. Interestingly, unless the order m is a multiple of 4 (e.g., $m = 0, \pm 4, \pm 8, \ldots$) the folding operation erases its ψ_d-dependent pattern,

$$\sum_{k=0}^{3} Y_{lm}(I,\psi_d + k\pi/2) \propto \sum_{k=0}^{3} \exp(imk\pi/2) = 0. \tag{12}$$

Correspondingly, the azimuthal patterns of the function $p(I,\psi_d)$ come only from $l \ge 4$.

As commented in Sec. II, an lth order pattern $Y_{l0}(\theta)$ in the original function Eq. (1) generates the term proportional to $L_l(\sin I \cos\psi)$ in the transformed one $p(I,\psi)$ in Eq. (5). From Eq. (2), we have

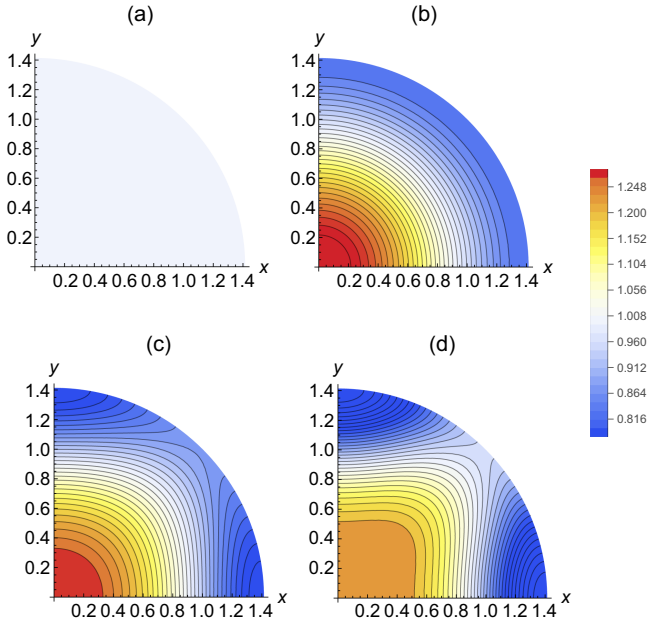

FIG. 2. The fourfolded orientation distributions $\bar{p}(I,\psi_d)$ (normalized by the factor π^{-1}). We apply the area preserving projection $(x,y)=2\sin(I/2)(\cos\psi_d,\sin\psi_d)$. The original distribution functions are axisymmetric model $\mathcal{P}_A(\cos\theta)$ in Eq. (1) characterized by the two anisotropy parameters a_{20} and a_{40}. Panel (a) for the isotropic model with $(a_{20},a_{40})=(0,0)$, (b) with $(-0.3,0)$, (c) with $(-0.3,-0.04)$, and (d) with $(-0.3,-0.1)$.

$$L_l[\sin I\cos\psi]+L_l[\sin I\cos(\psi+\pi)]=0,$$
$$L_l[\sin I\cos(\psi+\pi/2)]+L_l[\sin I\cos(\psi+3\pi/2)]=0,$$

for odd numbers l. Thus, the fourfolding operation (11) cancels out all the contributions from the odd-order patterns in Eq. (1).

Using Eqs. (5) and (11) and keeping the even orders $l\le 4$ we obtain,

$$\bar{p}(I,\psi_d)\propto Y_{00}-\frac{a_{20}}{2}Y_{20}(I)+\frac{3a_{40}}{8}Y_{40}(I)+\frac{a_{40}}{8}\left(\frac{35}{2}\right)^{1/2}[Y_{44}(I,\psi_d)+Y_{4-4}(I,\psi_d)],\quad(13)$$

which is symmetric at $I=\pi/2$. We should point out that the full function $p(I,\psi)$ [generated from Eq. (1) by Eq. (5)] has the components $Y_{2\pm2}(I,\psi)$, but they disappear at the folding operation as in Eq. (12) for $m=\pm2$.

In Fig. 2, we plot the folded distribution function (13) in the coordinate,

$$(x,y)=2\sin[I/2](\cos\psi_d,\sin\psi_d),\quad(14)$$

identical to the Lambert azimuthal equal-area projection centered on the face-on direction $I=0$. Given the symmetry at $I=\pi/2$, we present only the range $0\le I\le\pi/2$.

For a hierarchical case $|a_{20}|\gg|a_{40}|$, the azimuthal dependence is weak, as expected from Eq. (13). For $a_{20}<0$ [corresponding to the equatorial enhancement in Eq. (1)] we have higher probability around the face-on configuration ($I=0$ and π).

From the folded distribution function $\bar{p}(I,\psi_d)$, we can easily evaluate the polarization degree of the associated GW background. The Stokes parameters (I_s,Q_s,U_s,V_s) are its conventional measures [29,30]. Using the notation $\{\cdots\}_{\psi_d I}\equiv\int_0^\pi dI\int_0^{\pi/2}d\psi_d\sin I\bar{p}(I,\psi_d)[\cdots]$ for the angular averagings, we obtain the expressions such as

$$\frac{Q_s+iU_s}{I_s}=\frac{\{e^{-4i\psi_d}[(1+\cos^2 I)^2-4\cos^2 I]\}_{\psi_d I}}{\{[(1+\cos^2 I)^2+4\cos^2 I]\}_{\psi_d I}},\quad(15)$$

(defined for the axes $\vec{e}_r$ and $\vec{e}_q$). For the concrete profile (13), we have $Q_s/I_s=35a_{40}/(336-48\sqrt{5}a_{20}+3a_{40})$ and $U_s/I_s=V_s/I_s=0$.

IV. PROBING ANISOTROPIES

We now discuss how to probe the anisotropies of the original function $\mathcal{P}(\vec{j})$, by analyzing the observable function $\bar{p}(I,\psi_d)$, which is sampled by a finite number of CWDBs. For a probability distribution function defined on a sphere, following e.g., [31], we can deal with the discrete sampling effects on the spherical harmonic expansion. Here, paying attention to the roughly concentric profiles in Fig. 2, we rather examine a simple dualistic approach.

We divide our binary sample (in total N) into the following two subsets: (i) the low-inclination group with $|\cos I|\ge 1/2$ and (ii) the high-inclination group with $|\cos I|<1/2$. We put their numbers by N_L and N_H ($N_L+N_H=N$) and define the asymmetric ratio by

$$\mathcal{A}\equiv\frac{N_L-N_H}{N}.\quad(16)$$

For the isotropic (random) profile $\mathcal{P}(\vec{j})=$ const, we have the vanishing mean $\langle\mathcal{A}\rangle=0$ and the shot noise $\Delta\mathcal{A}=N^{-1/2}$ for the very basic binomial distribution. Below, we conservatively take the reference number $N\sim 2000$, considering the expected fraction of bulge CWDBs [14].

For an anisotropic profile $\mathcal{P}(\vec{j})$, we can estimate the mean fractions such as

$$\frac{\langle N_H\rangle}{N}=\int_{\pi/3}^{2\pi/3}dI\int_0^{\pi/2}d\psi_d\sin I\bar{p}(I,\psi_d),\quad(17)$$

and obtain

$$\langle\mathcal{A}\rangle=-\frac{192\sqrt{5}a_{20}+135a_{40}}{1024}\quad(18)$$

for the function (13). Therefore, if we have the condition $|\langle\mathcal{A}\rangle|>\Delta\mathcal{A}$, we can probe the intrinsic anisotropy in $\mathcal{P}(\vec{j})$

(at 1σ level). Dropping the term $\propto a_{40}$ in Eq. (18), the inequality can be expressed as

$$|a_{20}| > 0.053\left(\frac{N}{2000}\right)^{-1/2}. \tag{19}$$

This result would serve as a rough guidance for the detection limit of the intrinsic alignment of the bulge CWDBs.

We have some comments on the above simple arguments, in view of the selection effects at actual observational analysis. As shown in Eq. (6), the signal-to-noise ratio ρ depends on the sky position $\vec{n}$ of the binary and its orientation angles (I,ψ). For given parameters $(\vec{n},\psi)$, the signal-to-noise ratio ρ generally becomes smallest for an edge-on binary with $\cos I = 0$, as indicated by the expressions $A_{+,\times}(I)$. How about the dependence on the remaining parameters $(\vec{n},\psi)$ for edge-on binaries? In fact, due to the annual rotation of the detector plane of LISA, the dependence is effectively averaged out, and the associated scatter is largely suppressed. We can quantitatively examine this, by (i) using the standard framework for nearly monochromatic binaries with LISA-like detectors [16] and (ii) randomly sampling the parameters $(\vec{n},\psi)$. For an observational period of an integer times 1 yr, the minimum signal-to-noise ratio ρ of the edge-on binaries is only $\sim$10% smaller than the rms value of the whole edge-on sample (corresponding to the large number limit of detectors in [32]). In any case, the selection effect can be avoided by using CWDBs in the appropriate region in the $(f,\dot{f})$-space so that the Galactic survey is expected to be complete (e.g., $f > 3$ mHz) [11]. Alternatively, when preparing the binary sample, we can introduce dependence on the angular variables $(\vec{n},I,\psi)$ to the threshold of the signal-to-noise ratios.

Meanwhile, the estimation errors for the parameter $\cos I$ induce missclassifications of binaries around the boundary $|\cos I| = 1/2$, and we might need numerical studies to examine the potential biases for the asymmetric ratio $\mathcal{A}$. The Fisher matrix analysis roughly gives $\Delta\cos I \sim 1/\rho$ (except for $\cos I \sim \pm 1$) for a signal-to-noise ratio ρ (typically at $\sim$10–100 for a Galactic CWDB) [11]. Therefore, such confusions are relevant for a small fraction ($\sim 1/\rho$) of the binaries, eventually increasing the shot noise $\Delta\mathcal{A}$ only slightly (order of $N^{-1/2}\rho^{-1}$).

V. DISCUSSION AND SUMMARY

So far, we have mainly discussed the orientations of bulge CWDBs. Using LISA, from the ampluitude and frequency modulations, we can also measure the directions $\vec{n}$ of the binaries [16]. In addition, we will be able to estimate the distances to some of the inspiraling CWDBs by analyzing their orbital decay rates $\dot{f} > 0$ [17]. These pieces of positional information will help us to roughly select the bulge components. However, alignment studies will be intriguing also for disk components, and we do not need to stick too much with a separation between the two components. In any case, if the observed anisotropies $\bar{p}(I,\psi_d)$ are turned out to be strong, we could additionally explore the spatial correlation of the orientations, by combining the two- or three-dimensional positional information.

Let us briefly summarize our study. Compact binaries emit GWs, encoding their orbital motions. GW observation is intrinsically geometrical and enables us to measure the configurations of binary sources. Meanwhile, it was recently reported that, the orientations of the planetary nebulae associated with short-period bulge binaries are preferentially aligned to the Galactic plane, possibly reflecting the frozen initial conditions of the binaries [18]. In the near future, LISA will separately detect $\sim 10^4$ Galactic CWDBs and will become an ideal tool to examine their alignments, based only on the first principles of physics. In spite of the fourfold degeneracy of the polarization angles, LISA could enable us to measure the axisymmetric quadrupole pattern a_{20} as small as $\sim$0.05 and could serve as an interesting tool for geometrically delving into the fossil records in our Galaxy.

ACKNOWLEDGMENTS

The author would like to thank M. Iye and K. Tomida for valuable discussions. He also thanks K. Kyutoku and T. Tanaka for useful conversations.

[1] B. P. Abbott *et al.* (LIGO Scientific and Virgo Collaborations), Phys. Rev. Lett. **116**, 061102 (2016).
[2] B. P. Abbott *et al.* (LIGO Scientific and Virgo Collaborations), Phys. Rev. Lett. **119**, 161101 (2017).
[3] R. Abbott *et al.* (KAGRA, Virgo, and LIGO Scientific Collaborations), Phys. Rev. X **13**, 041039 (2023).
[4] G. Agazie *et al.* (NANOGrav Collaboration), Astrophys. J. Lett. **951**, L8 (2023).
[5] J. Antoniadis *et al.* (EPTA and InPTA: Collaborations), Astron. Astrophys. **678**, A50 (2023).
[6] D. J. Reardon, A. Zic, R. M. Shannon, G. B. Hobbs, M. Bailes, V. Di Marco, A. Kapur, A. F. Rogers, E. Thrane, J. Askew *et al.*, Astrophys. J. Lett. **951**, L6 (2023).
[7] H. Xu, S. Chen, Y. Guo, J. Jiang, B. Wang, J. Xu, Z. Xue, R. N. Caballero, J. Yuan, Y. Xu *et al.*, Res. Astron. Astrophys. **23**, 075024 (2023).

[8] P. Amaro-Seoane *et al.* (LISA Collaboration), Living Rev. Relativity **26**, 2 (2023).
[9] D. Hils, P. L. Bender, and R. F. Webbink, Astrophys. J. **360**, 75 (1990).
[10] S. Nissanke, M. Vallisneri, G. Nelemans, and T. A. Prince, Astrophys. J. **758**, 131 (2012).
[11] N. Seto, Phys. Rev. Lett. **128**, 041101 (2022).
[12] T. Kupfer, V. Korol, S. Shah, G. Nelemans, T. R. Marsh, G. Ramsay, P. J. Groot, D. T. H. Steeghs, and E. M. Rossi, Mon. Not. R. Astron. Soc. **480**, 302 (2018).
[13] T. Littenberg, N. Cornish, K. Lackeos, and T. Robson, Phys. Rev. D **101**, 123021 (2020).
[14] A. J. Ruiter, K. Belczynski, M. Benacquista, S. L. Larson, and G. Williams, Astrophys. J. **717**, 1006 (2010).
[15] E. Poisson and C. M. Will, *Gravity: Newtonian, Post-Newtonian, Relativistic* (Cambridge University Press, Cambridge, England, 2014).
[16] C. Cutler, Phys. Rev. D **57**, 7089 (1998).
[17] R. Takahashi and N. Seto, Astrophys. J. **575**, 1030 (2002).
[18] S. Tan, Q. A. Parker, A. A. Zijlstra, A. Ritter, and B. Rees, Astrophys. J. **951**, L44 (2023).
[19] K. B. Kwitter and R. B. C. Henry, Publ. Astron. Soc. Pac. **134**, 022001 (2022).
[20] N. Ivanova, S. Justham, X. Chen, O. De Marco, C. L. Fryer, E. Gaburov, H. Ge, E. Glebbeek, Z. Han, X. D. Li *et al.*, Astron. Astrophys. Rev. **21**, 59 (2013).
[21] T. C. Hillwig, D. Jones, O. De Marco, H. E. Bond S. Margheim, and D. Frew, Astrophys. J. **832**, 125 (2016).
[22] G. Duchêne and A. Kraus, Annu. Rev. Astron. Astrophys. **51**, 269 (2013).
[23] S. S. Huang and C. Wade, Astrophys. J. **143**, 146 (1966).
[24] J. Binney and M. Merrifield, *Galactic Astronomy* (Princeton University Press, Princeton, NJ, 1998).
[25] J. J. Sakurai and J. Napolitano, *Modern Quantum Mechanics* (Cambridge University Press, Cambridge, England, 2020).
[26] N. J. Cornish and S. L. Larson, Phys. Rev. D **67**, 103001 (2003).
[27] J. Roulet, S. Olsen, J. Mushkin, T. Islam, T. Venumadhav, B. Zackay, and M. Zaldarriaga, Phys. Rev. D **106**, 123015 (2022).
[28] R. Abbott *et al.* (LIGO Scientific and Virgo Collaborations), Phys. Rev. D **102**, 043015 (2020).
[29] G. B. Rybicki and A. P. Lightman, Radiative processes in astrophysics (1979), https://ui.adsabs.harvard.edu/abs/1986rpa..book.....R/abstract.
[30] J. D. Romano and N. J. Cornish, Living Rev. Relativity **20**, 2 (2017).
[31] S. Rao Jammalamadaka and Gyorgy H. Terdik, J. Multivariate Anal. **171**, 436 (2019).
[32] K. Yagi and N. Seto, Phys. Rev. D **83**, 044011 (2011); **95**, 109901(E) (2017).